PROCEEDINGS, 43rd Workshop on Geothermal Reservoir Engineering
Stanford University, Stanford, California, February 12-14, 2018
SGP-TR-213

Thermoelastic Analysis of Porous Media Using a Multiscale Asymptotic Expansion Homogenization Method

Mohammad Hatami, Levi Blake, Alireza Sarvestani, David Bayless

Department of Mechanical Engineering, Ohio University, Athens, OH 45701

bayless@ohio.edu

Keywords: Thermoelastic analysis, Porous medium, Finite element method, Asymptotic expansion homogenization, Multiscale simulation.

ABSTRACT

In this study, a multiscale finite element analysis coupled with the asymptotic expansion homogenization (AEH) method is employed to investigate the linear thermoelastic behavior of a porous medium. A stochastic method using a mixture of Gaussian functions distribution is used to generate microstructures. The simulated microstructures are produced based on the porosity of a Marcellus shale sample. The AEH method is used to determine the homogenized material properties of simulated random microstructures. A porous medium with material and transport properties that vary between the bedding layers and the matrix is generated. The influence of gas pressure, as well as thermal and mechanical loading on the porous medium is studied and the influence of the pore size and porosity of microstructures on the evolution of stress is investigated.

1. INTRODUCTION

Unconventional gas reservoirs are considered a significant energy source. The estimated recoverable natural gas in Marcellus shale alone is nearly 489 trillion cubic feet (Lora et al. (2016)). Unconventional reservoirs, namely shale, are significantly heterogeneous and porous materials with low permeability. The porosity of the rocks, along with the shape and size of the pore structures influence transport and mechanical properties of the shale. Experimental observations have demonstrated that the size of pore structures in the bedding layer is at least one order of magnitude larger than the pore size in the matrix (Arson et al. (2013)). Considering the importance of unconventional reservoirs, a fundamental study of core plug samples and porous microstructures subjected to mechanical and thermal loading, along with understanding the mechanical properties of rock samples are needed to advance techniques to increase the recovery of hydrocarbons beyond simple hydraulic fracturing.

The mineralogical compositions, such as mineral grains, pores, pore networks etc., have a strong influence on mechanical and transport properties. Gas flow in ultra-tight reservoirs is a multi-scale process controlled by the pore size and connectivity in the porous media (Fang (2017)). Theoretically, the gas flow regimes are classified based on the Knudsen number (Kn), defined as a ratio of the molecular mean free path to pore radius: continuum or Darcy flow ($Kn < 0.001$), slip flow ($0.001 < Kn < 0.1$), transition flow ($0.1 < Kn < 10$) and free molecular flow ($Kn > 10$) (Ray et al. (2003)). Once the probability of the gas molecules collision with pores wall is higher than that the gas molecules, the continuum assumption is no longer valid. Therefore, several models have been developed considering Knudsen diffusion and advection flow driven by pressure gradient (Javadpour (2009), Civan (2010), Darabi et al. (2012) and Kazemi et al. (2015)). Javadpour (2009) provided an analytical model for apparent permeability that considers the complexity of flow such that as average pore size decreases, the model converges to the Knudsen diffusion model and as average pore size increases, the model converges to the continuum model.

Determination of homogenized properties of polycrystalline rocks from a polished thin section of rock requires measuring crystallographic orientation of the minerals. The simplest and perhaps the most common methods to approximate the homogenized properties of heterogeneous media are the Voigt and Reuss bounds (Matthies and Humbert (1993) and Mainprice and Humbert (1994)). Single-particle approximations such as Mori-Tanaka and self-consistent methods constitute another class of homogenization techniques for determination of overall physical and thermo-mechanical properties of composite materials. The results of these analytical methods are generally in a close agreement with the available experimental data, however, the weakness of these methods is that they do not explicitly explain the influence of pores, grain shapes, grain distributions or grain-to-grain interactions.

Asymptotic expansion homogenization (AEH) is an advanced numerical method to evaluate a wide variety of physical and thermo-elastic properties of heterogeneous materials with microstructures (Bensoussan et al. (1978), Chung et al. (2001), Alzina et al. (2007), Zhang et al. (2007), Vel and Goupee (2010), Goupee and Vel (2010) and Naus-Thijssen et al. (2011b)). By decoupling the local (micro) and a global (macro) length scales, AEH is proved to be a computationally efficient tool to evaluate the continuum field quantities in a localized region of interest. The objective of this study is to present a multiscale finite element analysis coupled with an AEH method to predict the variation of macroscopic stresses in the porous structure of a shale sample. To this end, first a heterogeneous two-phase random microstructure is created based on the porosity of Marcellus shale and subsequently the homogenized thermoelastic material properties are estimated. The porous medium with material properties that vary between the matrix and bedding layers is constructed and the influence of gas pressure, thermal and mechanical loading on the porous medium is investigated. Also, the influence of pore size and porosity on stress distribution in the microstructure porous media is addressed.

2. SIMULATION OF RANDOM MICROSTRUCTURES

Figure 1 shows the structural details of shale at different length scales. The heterogeneous body consists of interconnected pores that are randomly distributed in a rock matrix. The representative material elements (RMEs) are generated to analyze the corresponding homogenized material properties of a rock sample. The length scale of RME is significantly small comparing to the macroscale length scale ($l << L$). The two length scales are related by the ratio of the RME size to the macroscopic body size ($\varepsilon = l / L$) which is assumed to be a small number.

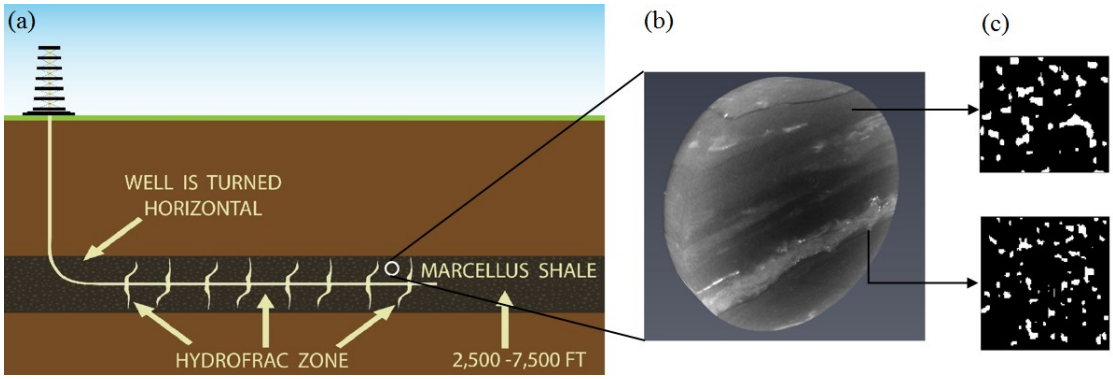

Figure 1: (a) Schematic visualization of large scale structure, (b) CT image of Marcellus shale sample, and (c) generated heterogeneous porous material with random pore structures.

Random morphology description functions (RMDFs) are used to generate microstructures similar to the Gaussian statistical field method, proposed by Robert and Teubner (1995). An RMDF is any arbitrary functions defined over a domain of interest to define the microstructural morphology. Assuming that the RME of interest occupies a domain designated by $Y = [0,l] \times [0,l]$, the RMDF is defined as a sum of two dimensional Gaussian functions over the region Y as

$$f(y) = \sum_{i=1}^{N} a_i e^{-\left[\frac{(y_1 - y_1^{(i)})^2 - (y_2 - y_2^{(i)})^2}{w_i^2}\right]} \tag{1}$$

$$w_i = \frac{l}{\sqrt{N}} \tag{2}$$

where N, a_i, y^i_1 , y^i_2 *and* w_i are the total number of Gaussian functions, values of random number chosen between -1 to 1, centers of Gaussian functions, and spatial widths of individual Gaussian functions, respectively. Figure 2 illustrates a sample RMDF generated over the domain Y with a random parameters a_i, y^i_1, y^i_2 and for $N = 800$. With increasing the number of Gaussian functions in (1), the number of voids with irregular shapes embedded in the microstructure increases.

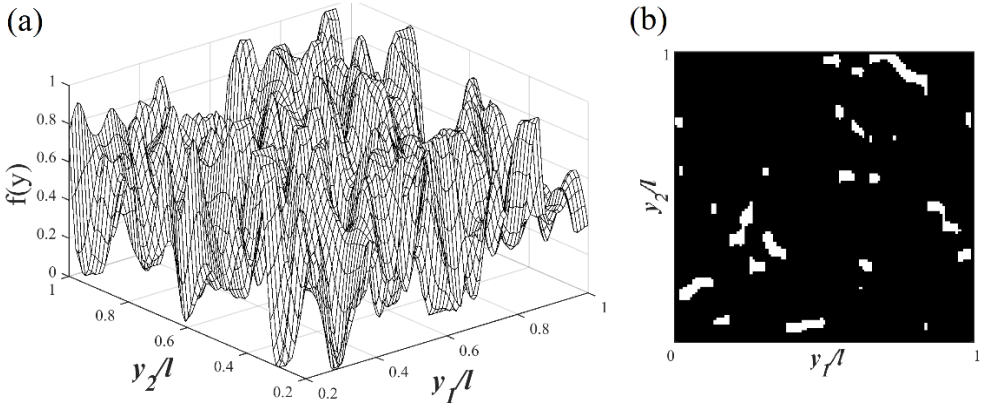

Figure 2: (a) Realization of an RMDF generated with $N = 800$, (b) Microstructure sample with 5% porosity.

Figure 3 shows microstructural morphologies corresponding to the RMDFs for several porosity data. By increasing the porosity, the voids interconnect across the width of RME.

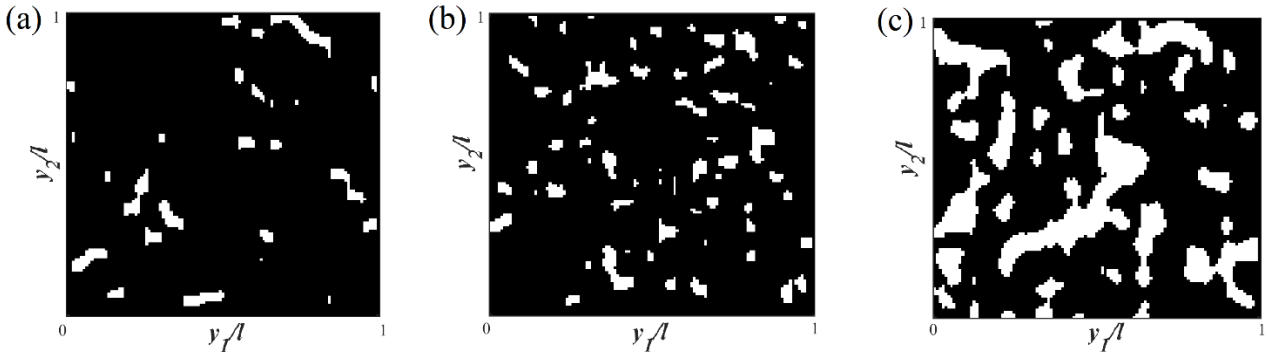

Figure 3: Microstructure porous media with (a) 5%, (b) 10%, and (c) 27%.porosities

3. MATHEMATICAL DESCRIPTION

In this section, the steady-state transport equations for gas flow with the gas molar mass M, gas viscosity μ and average gas density ρ in a porous medium with the porosity of ϕ are presented. Also, an overview of the AEH method for thermoelasticity problem is addressed.

3.1 Governing Equations

The steady state continuity equation for the gas flow can be presented as

$$\frac{\partial v_i^\varepsilon}{\partial x_i} = 0 \tag{3}$$

where v_i^ε is the velocity field that satisfies the Darcy's law

$$v_i^\varepsilon = \frac{k_{app}}{\mu}\frac{\partial p}{\partial x_i} \tag{4}$$

Here k_{app} and p are the apparent permeability and pressure, respectively. Darabi et al. (2012) have defined apparent permeability for a porous media considering the influence of the slip flow and Knudsen diffusion

$$k_{app} = \frac{\mu M}{RT_g \rho_{av}}\frac{\phi}{\tau}(\delta)^{D_f-2} D_k + k_D\left(1+\frac{b}{p}\right) \tag{5}$$

$$k_D = \frac{R_{av}^2}{8}\frac{\phi}{\tau} \tag{6}$$

$$b = \left(\frac{8\times 3.14\mathrm{RT_g}}{\mathrm{M}}\right)^{0.5}\frac{\mu}{R_{av}}\left(\frac{2}{\alpha_1}-1\right) \tag{7}$$

$$D_k = \frac{2R_{av}}{3}\left(\frac{8\mathrm{RT_g}}{3.14\mathrm{M}}\right)^{0.5} \tag{8}$$

where R is the gas constant, R_{av} is the average pore radius, τ is the tortuosity of the rock, D_f is the fractal dimension of the pore surface, k_D is the Darcy permeability, D_k is the Knudsen diffusion coefficient in porous media, δ is the ratio of normalized molecular size (d_m) to local average pore diameter (d_p), and α_1 is the tangential momentum accommodation coefficient (TMAC). Further, the steady state heat conduction and Fourier's law of heat conduction are defined by

$$-\frac{\partial q_i^\varepsilon}{\partial x_i} = 0 \tag{9}$$

$$q_i^\varepsilon = -\kappa_{ij}^\varepsilon \frac{\partial T^\varepsilon}{\partial x_j} \tag{10}$$

with T^ε being the difference in temperature from the reference state, q_i^ε the heat flux vector and κ_{ij}^ε as the thermal conductivity tensor. Finally, the equilibrium equation and the constitutive relations for the rock are

$$\frac{\partial \sigma_{ij}^\varepsilon}{\partial x_j} + f_i = 0 \tag{11}$$

$$\sigma_{ij}^\varepsilon = C_{ijkl}^\varepsilon e_{kl}^\varepsilon - \beta_{ij}^\varepsilon T^\varepsilon = C_{ijkl}^\varepsilon \frac{\partial u_k^\varepsilon}{\partial x_l} - \beta_{ij}^\varepsilon T^\varepsilon \tag{12}$$

where σ_{ij}^ε and f_i are the stress tensor and the body force per unit volume, respectively. The rock matrix is assumed to be a linear thermoelastic material with stiffness C_{ijkl}^ε and stress-temperature modulus e_{ij}^ε, β_{ij}^ε and u_k^ε stand for the infinitesimal strain tensor and displacement filed, respectively.

3.2 Asymptotic Expansion Homogenization Method

Only the key aspects of AEH method are recalled here, detailed descriptions can be found in Vel and Goupee (2010), Goupee and Vel (2010) and Naus-Thijssen et al. (2011b). Two length scales are considered for the AEH method, namely the macro-scale length *L* and the width *l* of the microstructure sample (as shown in Figure 1a). Terada et al. (2000) and Fish et al. (2000) showed that the so called boundary effect error due to implementation of displacement or traction boundary conditions vanished by consideration of a periodic boundary condition. In this work, a heterogeneous material is constructed based on the following assumptions: (1) any macroscopic domain is formed by periodic assembly of RME, (2) the solution is locally periodic, and (3) the macroscale fields remain constant within RME. The AEH method is valid for calculating the bulk elastic properties of the rock as long as the small heterogeneous scales are sufficiently small (more than three orders of magnitude) compared to the macroscale, such that response fluctuations due to the small scale heterogeneity is averaged out. The porous medium is constructed by spatial arrangement of a representative random microstructure (Figure 4). The RME is generated based on the statistical method presented in the previous section.

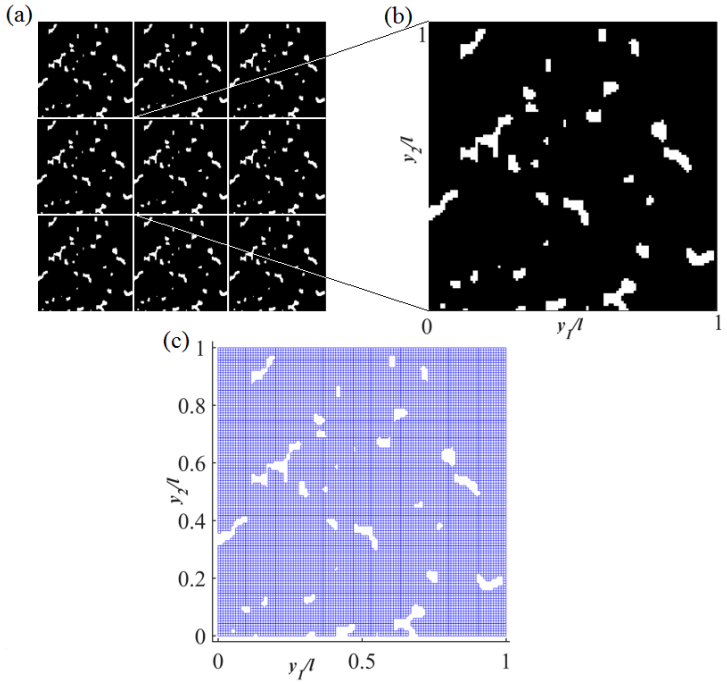

Figure 4: (a) The spatially periodic microstructure, (b) a porous RME, and (c) meshed RME for the finite element analysis.

The fluctuation of deformation at the micro level within the sample is proportional to the average macroscopic strains when the microstructure is subjected small deformations. The AEH method introduces characteristic functions χ_p^{kl} ***(y)*** that relate the microscale displacement fluctuations to the average macroscopic strains. The characteristic functions have the first-order correlation by considering microstructural features including the size, shape, elastic stiffness. The mechanical properties are determined using the characteristic functions and the spatially varying mechanical properties in the sample. The homogenized bulk stiffness tensor is defined as

$$C_{ijkl}^{H} = \frac{1}{|Y|}\int_{Y}\left(C_{ijkl}^{\varepsilon} - C_{ijpq}^{\varepsilon}\frac{\partial \chi_p^{kl}}{\partial y_q}\right)dY \tag{13}$$

where C^H_{ijkl} is the homogenized stiffness tensor. The first term in the integrand represents the Voigt bound and the second is a correction to the Voigt bound. The characteristic functions χ^{kl}_p ***(y)*** were determined using a finite element analysis on the RME subjected to periodic boundary conditions. For periodic boundary conditions, the number equations for nodes on the left and right and nodes on the top and bottom of the microstructure are equal. In order to satisfy the degrees of freedom, all four nodes at the corner of the microstructures are zero without any loss of generality.

4. DESCRIPTION OF COMPUTATIONAL MODEL

A core cylindrical sample with length L=100 *mm* and a diameter of D=50 *mm* placed in a typical permeability chamber is used for the multiscale analysis (Figure 5). The sample includes stacks of parallel thin bedding layers separating thicker matrix layers, as often observed in microscopic images of Marcellus shale. The random heterogeneous microstructures are generated throughout the porous medium by consideration of different porosity between bedding and matrix layers. The bedding layers with 2 *mm* thickness are placed in between 7 *mm* matrices with a porosity of 5*%*. Nitrogen gas is assumed to fill the pore for the purpose of permeability analysis. Due to the small difference in pressure across the sample, the mean pressure is considered for calculation of fluid properties and permeability. The material properties of Marcellus shale are listed in Table 1.

Table 1: Material properties of Marcellus shale sample (Lora et al. (2016), Darabi et al. (2012)).

Young's modulus (E)	18 *GPa*
Poisson's ratio (υ)	0.15
Thermal conductivity (κ)	1.8
Thermal expansion coefficient (α_T)	2.6×10^{-6} (K^{-1})
Porosity (ϕ, matrix and bedding layers)	5 and 10 %
Fractal dimension of the pore surface (α_1)	2.2
Tortuosity (τ)	2
TMAC	0.9
Average pore radius (R_{av})	10 (nm)
Temperature (T)	300 (K)

The porous medium is subjected to a uniform distributed confining pressure (σ_c=20 *MPa*), the upstream and downstream pressures for gas flow are 6 and 4 *MPa*, respectively. A uniform temperature of T_c=350 *K* is applied on its upper and lower surfaces whereas both ends of the sample are kept at a constant temperature T_s=300 *K*. The gas flow is assumed to be in one dimension along the length of the sample. Due to the symmetry in geometry, only a half of the domain is analyzed. The origin of the global Cartesian coordinate system is attached to the left corner of the plane of symmetry (Figure 5) and a two-dimensional plane strain analysis is performed at the macroscopic level.

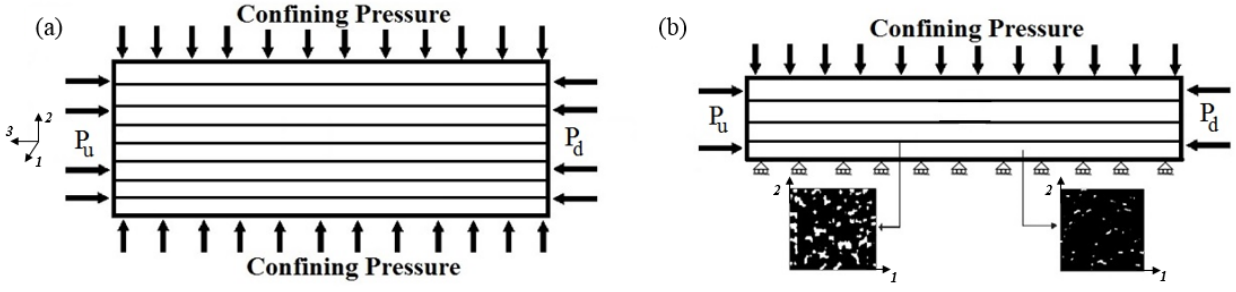

Figure 5 (a-b): Schematic diagram of core sample with parallel bedding layers and assumed boundary conditions.

5. RESULTS

At the first step, the AEH method is used to determine the homogenized material properties at each layer. Figure 6 shows the results of a convergence analysis to find the thermal conductivity κ^H, thermal expansion coefficient α_T^H, and Young's modulus E^H of matrix layer with increasing the number of elements N_e. Four-node quadrilateral elements are used to generate the mesh into the microstructure porous medium. The number of elements is normalized by the number of Gaussian functions N used to create the random microstructure (as shown in Figure 4c). As expected, with increasing the number of elements and capturing the complexity of microstructural morphology of the porous medium the homogenized material properties converge to a unique value. The numerical results show that the homogenized material properties converge at the ratio $\sqrt{N_e / N}$ equal to 3 or larger. $\sqrt{N_e / N} = 3.9$ is selected for the studies presented here. The homogenized material properties of different layers of porous medium are listed in Table 2.

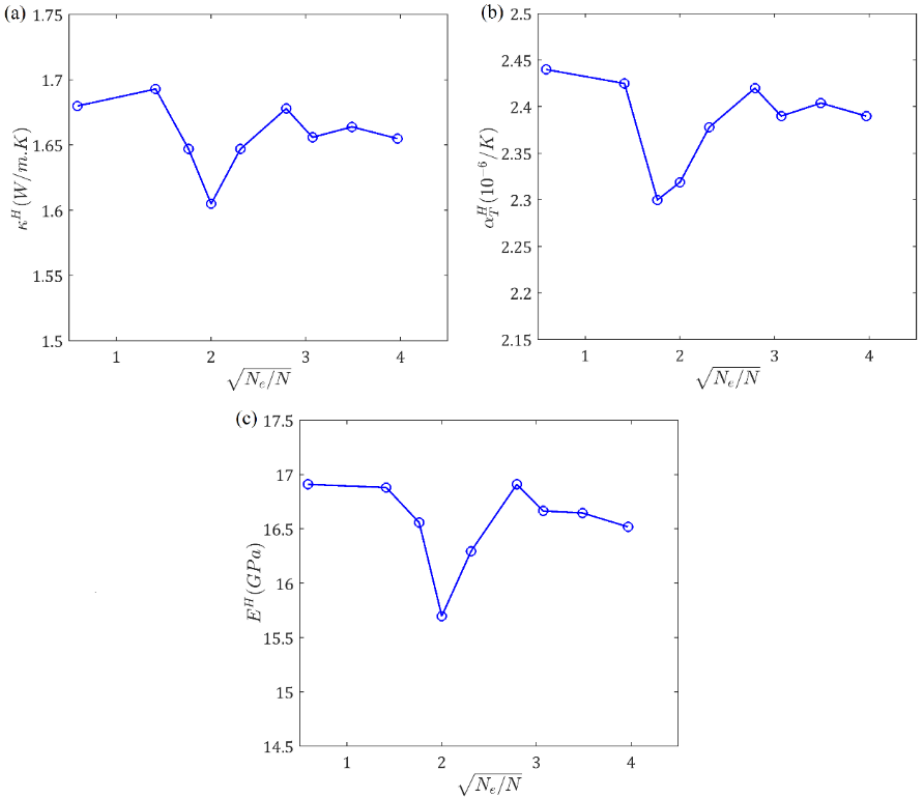

Figure 6: Convergence analysis of homogenized (a) thermal conductivity, (b) thermal expansion coefficient, and (c) Young's modulus.

Table 2: Homogenized material properties of Marcellus shale sample.

	Matrix ϕ=5%	Bedding layer ϕ=10%
Young's modulus (E^H)	17.05 *GPa*	15.15 *GPa*
Poisson's ratio (υ)	0.15	0.15
Thermal conductivity (κ^H)	1.656 ($W/m.K$)	1.478 ($W/m.K$)
Thermal expansion coefficient ($\alpha^H{}_T$)	2.39×10^{-6} (K^{-1})	2.136×10^{-6} (K^{-1})
Apparent permeability (k_{app})	2.1245×10^{-13} (m^2)	4.2491×10^{-12} (m^2)

At the next step, the distribution of different thermoelastic field quantities are evaluated in the porous medium. The domain is discretized using a total of 8000 four-node quadrilateral elements. The distribution of gas pressure in the porous medium is shown by Figure 7. The lateral sides of core holder are assumed to be impermeable and therefore, the gas pressure uniformly changes along the length of the porous medium. Similar results are presented by Naraghi and Javadpour (2015) and Sun et al. (2011b). The apparent permeability in the bedding layer and the matrix are found to be 4.2491×10^{-12} m^2 and 2.1245×10^{-13} m^2, respectively.

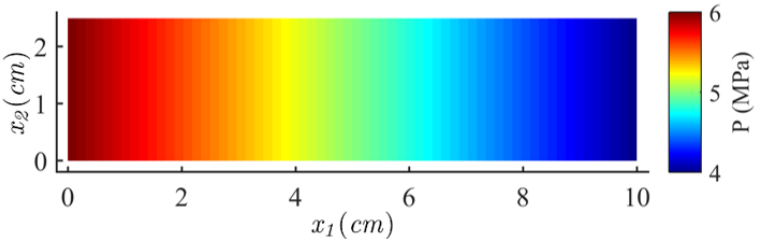

Figure 7: Pressure distribution of the steady-state fluid flow of the porous medium.

Figure 8a shows the macroscopic temperature distribution in the porous medium. The thermal conductivity of the bedding layers is lower than the matrices as a result of higher porosity and larger fraction of empty spaces that act as thermal insulators. Therefore, temperature drop is more significant in the bedding layer in comparison with that in the matrix. The spatial variation of macroscopic components of stresses (σ_{11}, σ_{22} and σ_{12}) are depicted in Figure 8b-d. The pressure field induced by the gas flow and is transferred to the boundary of the porous medium. The critical locations are on both ends of the middle region of the porous medium and the peak stresses are found to be $\sigma_{11} = 266.78\ MPa$ and $\sigma_{22} = 25.21\ MPa$.

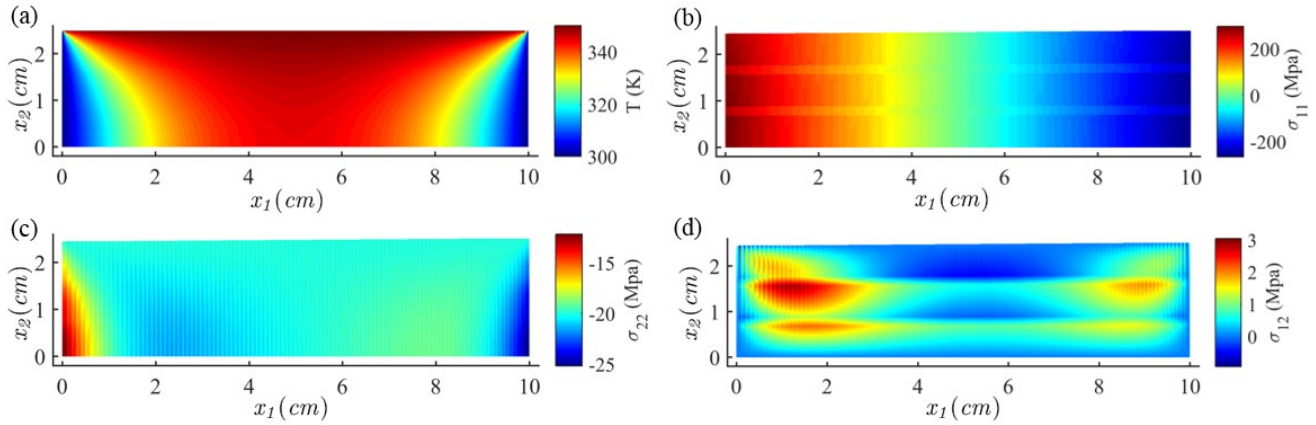

Figure 8: Contour plots of (a) temperature and macroscopic stress components (b) σ_{11} , (c) σ_{22} , and (d) σ_{12} .

Two specific microstructures with porosities of 5% and 10% at the right corner of symmetry plane (subjected to compressive stresses) are selected for micromechanical studies. The micro stresses $\sigma_{11}^0, \sigma_{22}^0$ and σ_{12}^0 corresponding to the microstructures with porosities of 5% and 10% are shown in Figure 9a-f. The average pore diameters slightly decrease in response to a compressive loading. As porosity increases from 5% in the matrix to 10% in the bedding layer, the magnitudes of micro stresses increase almost by one order of magnitude. In the bedding layers with 10% porosity, localized bands of highly stressed regions are formed that connect the pores. In addition, the concentration of micro stresses around the packed pore structures is considerably higher than the rest of the matrix.

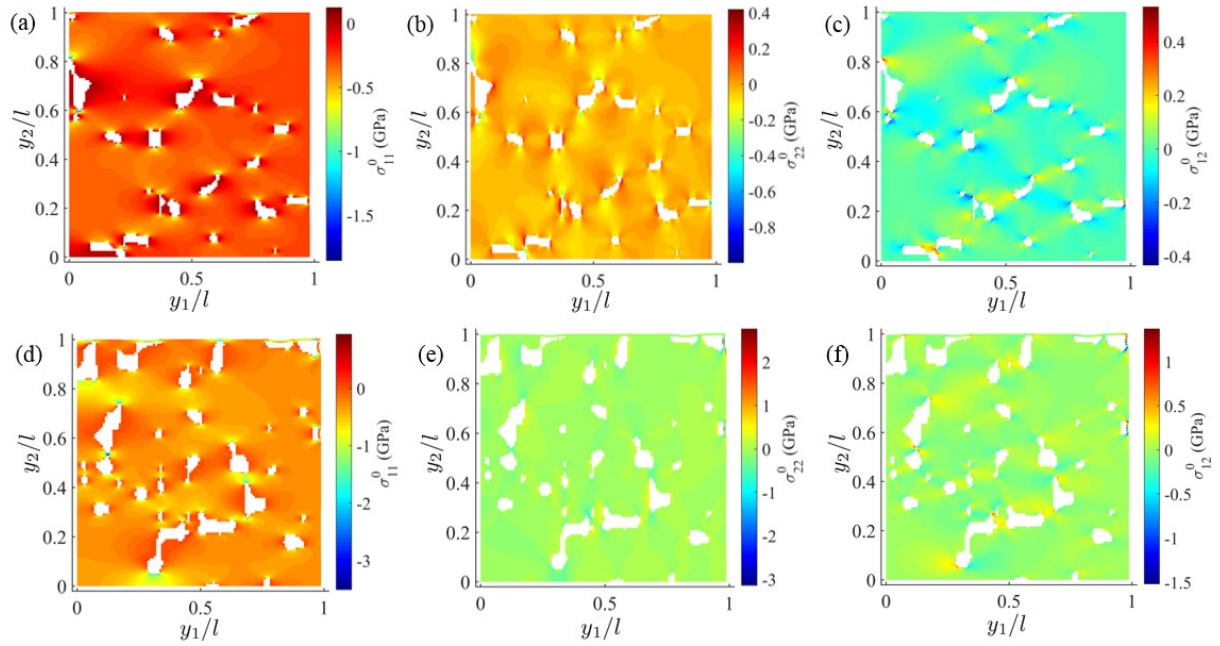

Figure 9: Contour plots of microscopic stress components (a) σ_{11}^0, (b) σ_{22}^0, and (c) σ_{12}^0 for microstructure with 5% porosity and (d) σ_{11}^0, (e) σ_{22}^0, and (f) σ_{12}^0 for microstructure with 10% porosity.

Figures 10a-f show the microscopic stress distribution σ_{11}^0 in several microstructure realizations while the porosity is considered to be constant and equal to 10%. The microstructure are located at the right corner of the symmetry plane. Again, the results show that the pore arrangement is a dominant factor in determination of micro stress distribution. A band of areas with high concentration of stress (and strain) is formed between the adjacent pore structures. It is anticipated that such localized deformation significantly reduces the strength of the whole porous medium and leads to material failure.

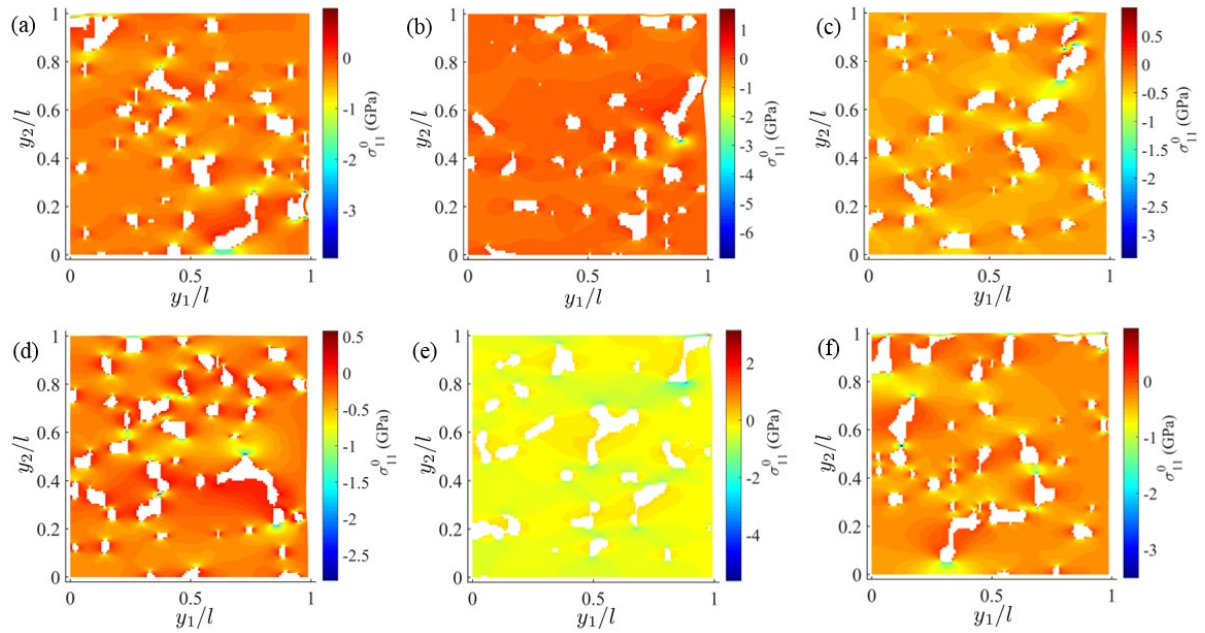

Figure 10: Contour plots of microscopic stress component σ_{11}^0 for several microstructure realizations (a-f) with 10% porosity in a bedding layer.

Figure 11 shows the microscopic stress distribution σ_{11}^0 in the microstructures with a constant porosity of 10% while the number of pore structures has been increased by changing the number of Gaussian functions. Increasing the number of Gaussian functions results in decreasing the pore size while the porosity remains constant. As the number of pore structures increases, localized bands of regions with high intensity of micro stresses are formed between the pores. Moreover, the irregular shape and the orientation of pore structures show a significant effect on the micro stress evolution in the porous media.

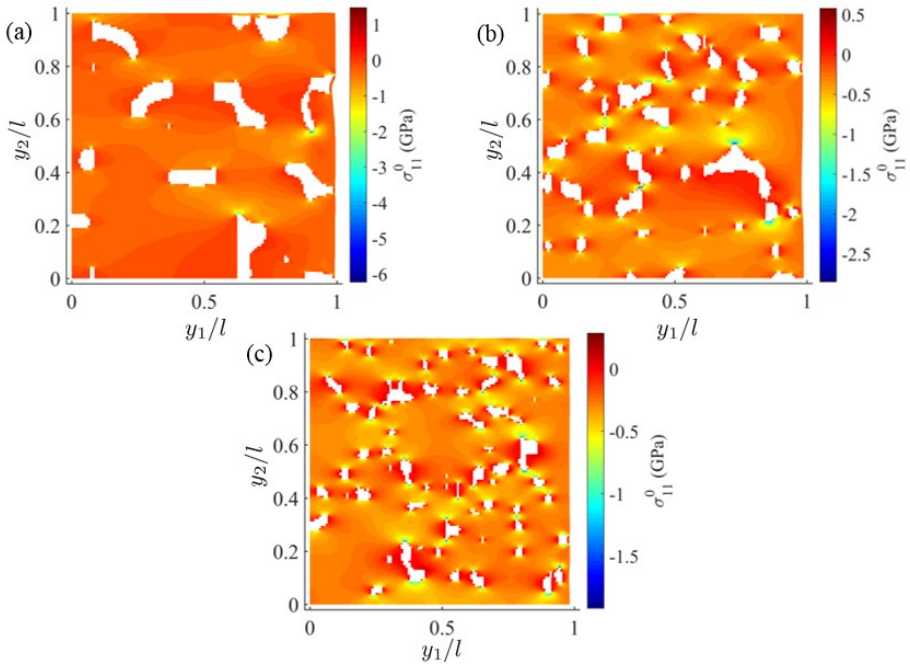

Figure 11: Contour plots of microscopic stress component σ_{11}^0 for microstructures with 10% porosity in a bedding layer and (a) *N=400*, (b) *N=800*, and (c) *N=2500*.

6. CONCLUSIONS AND RECOMMENDATIONS

A multiscale computational methodology is introduced to analyze the distribution of stress in heterogeneous microstructure of Marcellus shale. Random porous microstructures are generated with porosities comparable with the results of microscopic imaging on shale samples. The homogenized material properties are determined using AEH method. A finite element discretization scheme coupled with AEH is used to compute the field variables, including the gas pressure and different components of stress. It is demonstrated that the apparent permeability of the bedding layer is more than that of the matrix. Within the range of elastic deformations, the permeability of shale sample decreases in response to the applied compressive loading. Thermal properties of microstructures appear to be weak in the bedding layers comparing to those in the matrix and heat is essentially transferred via the rock matrix. In high porosity microstructures, the highest micro stresses occur in regions where the pores are closely spaced and form a narrow localized bands connecting the adjacent pores. Pore density is a dominant factor for localization of micro stress and damage is likely to occur between the packed pores. The irregular shape and the orientation of pore structures have a significant effect on the microscopic stresses in the porous media.

ACKNOWLEDGEMENT

This work was supported by Ohio University's Innovation Strategies Program # 40613 and funding from the Russ College of Engineering.

REFERENCES

Lora, R.V., Ghazanfari, E., and Izquierdo E.A.: Geomechanical Characterization of Marcellus Shale. *Rock Mech and Rock Eng*, **49**, (2016), 3403-3424.

Arson, C., and Pereira, J.M.: Influence of damage on pore size distribution and permeability of rocks. *International Journal for Numerical and Analytical Methods in Geomechanics*, **37**, (2013), 810-831.

Fang, Z.: An Improved Method of Permeability Estimation Based on Pulse-Decay Experiment Using Illinois Coal. The Pennsylvania State University, Pennsylvania, (2017).

Roy, S., Raju, R., Chuang, H.F., Cruden, B.A., and Meyyappan, M.: Modeling gas flow through microchannels and nanopores. *J. Appl. Phys.*, **93**, (2003), 4870-4879.

Javadpour, F.: Nanopores and apparent permeability of gas flow in mudrocks (shales and siltstone). *J. Can. Pet. Technol.*, **48**, (2009), 16-21.

Civan, F.: Effective correlation of apparent gas permeability in tight porous media. *Transp. Porous Media,* **82**, (2010), 375-384.

Darabi, H., Ettehad, A., Javadpour, F., and Sepehrnoori, K.: Gas flow in ultra-tight shale strata. *J. Fluid Mech.*, **710**, (2012), 641-658.

Kazemi, M., and Takbiri-Borujeni, A.: An analytical model for shale gas permeability. *Int. J. Coal Geol.*, **146**, (2015), 188-197.

Matthies, S., and Humbert, M.: The realization of the concept of a geometric mean for calculating physical constants of polycrystalline materials. *Phys. Status Solidi B-Basic Solid State Phys*., **177**, (1993), K47-K50.

Mainprice, D., and Humbert, M.: Methods of calculating petrophysical properties from lattice preferred orientation data. *Surv. Geophys*., **15**, (1994), 575-592.

Bensoussan, A., Lions, J.L., and Papanicolau, G.: Asymptotic Analysis for Periodic Structures. North-Holland, Amsterdam, (1978).

Chung, P.W., Tamma, K.K., and Namburu, R.R.: Homogenization of temperature dependent thermal conductivity in composite materials. *AIAA J Thermophys. Heat Transf*, **15**, (2001), 10-17.

Alzina, A., Toussaint, E., and Béakou, A.: Multiscale modeling of the thermoelastic behavior of braided fabric composites for cryogenic structures. *Int. J. Solids Struct.*, **44,** (2007) 6842-6859.

Zhang, H.W., Zhang, S., Bi, J.Y., and Schrefler, B.A.: Thermo-mechanical analysis of periodic multiphase materials by a multiscale asymptotic homogenization approach. *Int. J. Numer. Methods Eng.*, **69**, (2007), 87-113.

Vel, S.S., and Goupee, A.J.: Multiscale thermoelastic analysis of random heterogeneous materials. Part I. Microstructure characterization and homogenization of material properties. *Computational Materials Science*, **48**, (2010), 22-38.

Goupee, A.J., and Vel S.S.: Multiscale thermoelastic analysis of random heterogeneous materials. Part II. Direct micromechanical failure analysis and multiscale simulations. *Computational Materials Science*, **48**, (2010), 39-53.

Naus-Thijssen F.M.J., Goupee A.J., Vel S.S., and Johnson S.E.: The influence of microstructure on seismic wave speed anisotropy in the crust: Computational analysis of quartz-muscovite rocks. *Geophys. J. Int.*, **185**, (2011b), 609-621.

Roberts A.P., and Teubner M.: Transport properties of heterogeneous materials derived from Gaussian random fields: Bounds and simulation. *Physical Review E*, **51**, (1995), 4141-4154.

Terada, K., Hori, M., Kyoya, T., and Kikuchi, N.: Simulation of the multi-scale convergence in computational homogenization approaches. *Int. J. Solids Struct.*, **37**, (2000), 2285-2311.

Fish, J., and Shek, K.: Multiscale analysis of composite materials and structures. *Comput. Sci. Technol*, **60**, (2000), 2547-2556.

Naraghi, M.E., and Javadpour F.: A stochastic permeability model for the shale-gas systems. *Int. J. Coal Geol.*, **140**, (2015), 111-124.

Sun, W.C., Andrade, J.E., and Rudnicki, J.W.: Multiscale method for characterization of porous microstructures and their impact on macroscopic effective permeability. *J. Numer. Methods Eng.*, **88**, (2011b), 1260-1279.